
In-situ pull-out tests on soil-reinforcement interface properties of reinforced soil slopes

Cunjia Qiu^{1,2,*}, Shuang Wang², Hong Liu³, Jin Huang²

1. College of Environment and Civil Engineering,
Chengdu University of Technology, Chengdu 610059, China
2. Southwest Branch of China Airport Construction Group Company Limited,
Chengdu 610202, China
3. Key Laboratory of Karst Environment and Geohazard Prevention,
Ministry of Education, Guizhou University, Guiyang 550003, China
994077512@qq.com

ABSTRACT. In recent years, geogrid materials have been widely adopted for high fill slopes of airports in mountainous regions, as they can cope with the heavy earth/stonework, high filling height, complex filler properties and diverse topography. The properties of the soil-reinforcement interface (SRI) between geogrids and fillers directly bear on the safety of the reinforced structure. To improve the design of reinforced soil structure, it is imperative to determine the SRI properties in in-situ states, disclose the load transmission law, and identify the effective length of reinforcement strip. This paper carries out in-situ pull-out tests on the high fill slopes of an airport, explores the in-situ pull-out properties of geogrids under long-term, large-scale earth/stonework construction, and analyses the variation laws of parameters like strain, stress and displacement under different pull-out forces. Assuming that the relationship between strain and position is an S-curve, the theoretical relationships between these parameters and geogrid position were derived. Through the comparison against the test results, it is proved that the S-curve model outputted basically the same laws with those observed in the tests. The research findings provide a valuable reference for the design of reinforced soil structure.

RÉSUMÉ. Ces dernières années, les matériaux de géogrid ont été largement adoptés pour les pentes de remblayage des aéroports dans les régions montagneuses, car ils peuvent supporter des sols lourds et le maçonnerie, une hauteur de remplissage élevée, des propriétés de remplissage complexes et une topographie variée. Les propriétés de l'interface de renforcement de sol (SRI en anglais) entre les géogrids et les matériaux de remplissage ont une incidence directe sur la sécurité de la structure renforcée. Pour améliorer la conception de la structure de sol renforcée, il est impératif de déterminer les propriétés de l'interface de consolidation de sol dans les états in situ, de divulguer la loi de transmission de la charge et d'identifier la longueur effective de la bande de renforcement. Cet article effectue des tests en retrait in situ sur les pentes de remplissage d'un aéroport, explore les propriétés de retrait in situ des géogrids dans le cadre de la construction à long terme de terres et de maçonnerie, et

analyse les lois de variation de des paramètres tels que la déformation, la tension et le déplacement sous différentes forces de retrait. En supposant que la relation entre la déformation et la position soit une courbe en S, les relations théoriques entre ces paramètres et la position de la géogrid ont été dérivées. La comparaison avec les résultats des tests a montré que le modèle à courbe en S produisait essentiellement les mêmes lois que celles observées dans les tests. Les résultats de la recherche fournissent une référence précieuse pour la conception de la structure de sol renforcée.

KEYWORDS: reinforced soil slope, geogrid, in-situ pull-out test, soil-reinforcement interface (SRI), s-curve.

MOTS-CLÉS: pente de sol renforcé, géogrid, test en retrait in situ, interface de renforcement de sol, courbe en S.

DOI:10.3166/ACSM.42.41-56 © 2018 Lavoisier

1. Introduction

The stability of high fill slope is a core technical issue in airport construction in Southwest China. In this region, the airports are often built on high fill slopes, which require extensive land levelling over various geological units. The construction of such an airport faces significant changes in stratum and complex conditions of topography, geology and groundwater occurrence. All these factors, coupled with the lack of diverse fillers, make it difficult to ensure slope stability (Liu *et al.*, 2004).

To solve the problem, geosynthetics have been widely applied in the construction of high fill airports. The performance of reinforced soil structures, an important type of geosynthetics, depends heavily on such properties of the soil-reinforcement interface (SRI) as the mechanical law, the strength parameter (Wang *et al.*, 2016), the load transfer law (Wang *et al.*, 2016) and the variation patterns of strain and displacement (Chen and Li, 2009). These properties are essential to the design of reinforced soil slopes.

Much research has been done on the performance of reinforced soil structures. For example, Chen *et al.* (2009) carried out an indoor pull-out test to identify the distribution features of the SRI friction. Through indoor pull-out test and theoretical analysis, Wang *et al.* (2016) and Yang *et al.* (2013) examined the distribution features of the axial force of the reinforcement strip. From an indoor test, Liu *et al.* (2013) derived the formulas for the tensile force distribution along the reinforcement and for the relative displacement between soil and reinforcement at each point. Wang *et al.* (2016), Shi *et al.* (2009), Meng and Xu (2009) and Bakeer *et al.* (1998) investigated the shear strengths of various geotechnical materials and fillers through indoor direct shear test or indoor pull-out test. In the above studies, the SRI properties are explored through indoor direct shear test or indoor pull-out test. However, the scale of indoor tests is too small to yield close-to-reality test parameters and deformation features.

Compared with indoor tests, the large-scale in-situ pull-out tests are suitable to disclose the actual working states of reinforced soil. For example, Zhang (2008), Yang *et al.* (2009), Mo *et al.* (2008) and Liu *et al.* (2011) studied the distribution features of the pressure and reinforcement strain in reinforced soil retaining walls

under in-situ working conditions. Nevertheless, these studies are limited to the soil pressure distribution of reinforced soil retaining walls. There is no report yet on the SRI properties of reinforced soil slopes, not to mention those of airports with heavy earthwork and complex fillers. What is worse, the in-situ tests are rarely adopted in engineering projects because they are too time-consuming and costly. To improve theories on reinforced soil structure and guide the design of reinforced soil slope, it is imperative to clarify the SRI properties of reinforced soil slope in the in-situ states.

In this paper, steel-plastic geogrid and steel-plastic tenon geogrid, which are commonly used in airport high-filling engineering, are selected for large-scale in-situ pull-out tests of reinforced soil slopes in Liupanshui Airport. In this region, the fillers are mainly carbonaceous mudstones. Through these tests, the author obtained the variation laws of strain and pull-out displacement of the geogrids under the in-situ states. After that, the relationship between strain and position at any state was simulated with the S-curve model. The results show that this empirical model can basically reflect the SRI properties under any pull-out force. The research findings provide a valuable reference for the design of reinforced soil slopes.

2. Materials and parameters

2.1. Geogrids

Two geogrids were adopted for our tests, namely, steel-plastic geogrid and steel-plastic tenon geogrid. The main technical parameters of the geogrids are listed in Table 1, where the strength and strain are the mean measured value. It can be seen from the table that the two geogrids share the same geometrical dimensions and strength features, except the tenon part. The coverage of steel-plastic geogrid and that of steel-plastic tenon geogrid was set to 19.02% and 19.04%, respectively.

Table 1. Main technical parameters of geogrids

| Type of material | Rib strip length | Barrier strip length | Rib strip width | Barrier strip width | Rib strip thickness | Barrier strip thickness | Material density | Peak strain | Single-rib peak strength | Single-rib strength at 2% strain |
|-----------------------------|--------------------|----------------------|--------------------|---------------------|---------------------|-------------------------|-------------------|-------------|--------------------------|----------------------------------|
| | L ₁ /mm | L ₂ /mm | d ₁ /mm | d ₂ /mm | d ₁ /mm | d ₂ /mm | g/cm ³ | % | kN | kN |
| Steel-plastic tenon geogrid | 200 | 150 | 18 | 18 | 2.5 | 2.5 | 1.0 | 3.21 | 11.43 | 10.15 |
| Steel-plastic geogrid | 200 | 150 | 18 | 18 | 2.5 | 2.5 | 1.0 | 2.98 | 11.32 | 10.35 |

2.2. Fillers and properties

The fillers are fragmented stones and soils collected from the Liupanshui Airport test area. The content of block stones is about 10%~30%. The collected stones are mostly carbonaceous mudstone and sand mudstone, plus a few limestone and dolomite. The main mechanical parameters of the fillers were determined through field sampling and lab tests (Table 2). The parameters of the interface between each type of geogrid and the fillers were obtained through separate indoor pull-out tests. The test results show that the internal friction angle and the cohesion between steel-plastic geogrid and the fillers were 26.2° and 5.55kPa, respectively, while those between steel-plastic tenon geogrid and the fillers were 27.81° and 10.24kPa, respectively.

Table 2. Main mechanical parameters of the fillers

| Characteristic index | Test value | Characteristic index | Test value | Characteristic index | Test value |
|--|------------|--|------------|---|------------|
| Density (g/cm ³) | 2.21 | Curvature coefficient C _c | 2.12 | Controlled particle size d ₁₀ (mm) | 0.42 |
| Specific gravity of soil particle G _s | 2.681 | Maximum dry density (g/cm ³) | 2.21 | Unevenness coefficient C _u | 42.86 |
| Optimal water content (%) | 9.51 | c/kPa | 2.60 | $\varphi/^\circ$ | 32.41 |

3. In-situ pull-out tests

3.1. Test plans

The in-situ pull-out tests were carried out in the filling area of Liupanshui Airport. The filling area was divided into two test areas. As shown in Figure 1, test area A lies on the third-level berm (thickness of overlying soil layer: 25m; mean slope ratio: 1:2.2), while test area B lies on the second-level berm (thickness of overlying soil layer: 12m; mean slope ratio: 1:2.0).

As mentioned before, the fillers in the test areas are fragmented stones and soils. The content of block stones is about 10%~30%. The collected stones are mostly carbonaceous mudstone and sand mudstone, plus a few limestone and dolomite.

The geogrids were laid in two layers, with a vertical spacing of 60cm. The geogrids were 30m~40m in length and 2m in width. All geogrids were numbered according to the type and the thickness of the overlying soil layer. Taking test area A for example, the geogrids A1~A4 were arranged in the lower row, while the geogrids A5~A8 were arranged in the upper row. The geogrid arrangement in test

area B is the same as that in test area A. The test plan for each number is shown in Table 3.

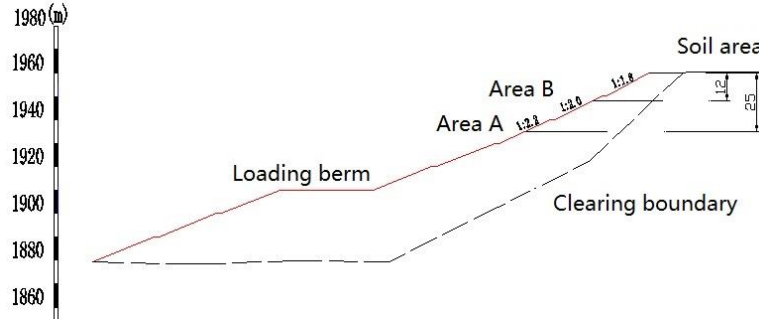


Figure 1. Areas for pull-out tests

Table 3. Pull-out test areas

| Test area | Soil thickness(m) | Tenon geogrid | Non-tenon geogrid |
|-----------|-------------------|---------------|-------------------|
| A | 25 | A1, A3 | A2, A4 |
| | 24.4 | A5, A7 | A6, A8 |
| B | 12.0 | B1, B3 | B2, B4 |
| | 11.4 | B5, B7 | B6, B8 |

3.2. Test devices and procedures

The test devices mainly include a tension system, a reaction device and a test device (Figure 2). Among them, the tension system consists of a jack, a force-transmitting rod and a fixture; the reaction device is a cast-in-situ T-shaped reaction wall (cross-section size: 2.5m×2m; length: 8m). During the tests, the pull-out displacement was measured by a large-scale dial gauge, the strain was captured by BX120-4AA foil acetal strain gauges. The tests were implemented in the following steps:

- (1) Preparations: Prepare the various devices and materials required for the tests. The geogrids must be stored in shady places.
- (2) Land levelling: Clean and level the surface of the soil layer to be paved with geosynthetics. No hard protrusions (e.g. broken and block stones) are allowed on the surface.
- (3) Geogrid pavement: Perform surveying and setting out, lay the geogrids to the pre-set positions according to the specified length (Figure 3), paste the strain gauges

(Figure 4) and carry out protection treatment. This step should be implemented by the measuring personnel.

(4) Filler application: Apply the fillers and roll them layer by layer to the designed elevation.

(5) Slope trimming: Trim the slope and build the reaction wall.

(6) Pull-out tests: Install the test devices, apply a 10kN preload, and record the pull-out displacement and strain; after that, increase the load by 10kN each time until the geogrids are damaged.

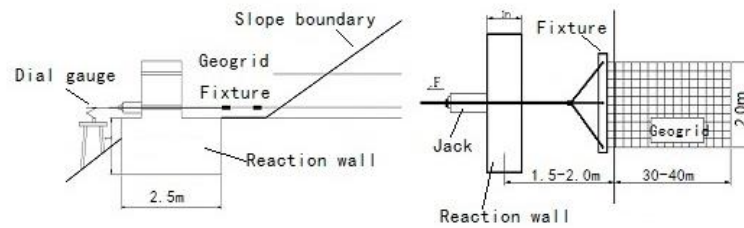


Figure 2. Test devices and plans for in-situ pull-out tests



Figure 3. Geogrid arrangement

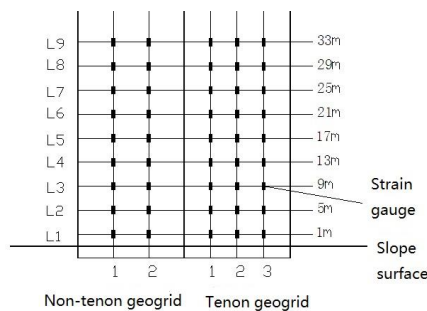


Figure 4. Layout of strain gauges

4. Test results

The test in test area A was carried out 7~8 months after the pavement of the geogrids, and that in test area B was conducted 3 months after the pavement. During the tests, 96 out of the 126 strain gauges installed in test area A were damaged, putting the damage rate at 76%; 136 out of the 168 strain gauges installed in test area B were damaged, putting the damage rate at 81%. Thus, the measured strain only partially demonstrates the deformation of geogrids in the pull-out process. The main results of the tests are as follows:

(1) Figure 5 presents the relationship curve between pull-out force and pull-out displacement. It can be seen that the pull-out displacement changed almost linearly with the pull-out force. The displacement exhibited a near-linear increase with the growth in pull-out force, when the latter was smaller than 58kN. However, the displacement increased nonlinearly with the growth in pull-out force, when the latter was greater than 58kN.

(2) Figure 6 shows the relationship between the strain of each part of the geogrid and the pull-out force. In general, the strain increased with the pull-out force. In test area A, the strain was roughly linear with the pull-out force; in test area B, the strain increased with the pull-out force in an oscillatory manner. A possible reason for the difference goes as follows: the overlying soil layer in test area B was thinner than that in test area A and had not fully consolidated in the relatively short period (3 months); as the pull-out force increased in the test, the stress was redistributed due to the slip of the SRI, resulting in a slight reduction in geogrid strain.

(3) Figure 7 depicts the relationship between strain and geogrid position in the in-situ tests. A monotonous decreasing relationship can be found between the two factors, that is, the geogrid deformation is negatively correlated with the distance to the slope surface. However, the relationship between the two factors is so complex that different variation laws were observed in different tests. In test area A, the strain decreased almost linearly along the tensile direction: the geogrid deformation was obviously reduced after the geogrid length surpassed 13m and was relatively small after the geogrid length exceeded 17m (where the strain was less than 1%); the strain dropped to zero when the geogrid length surpassed 21m. In test area B, the steel-plastic tenon geogrid (B7) had basically the same strain at all positions when its length was shorter than 9m; the deformation was reduced drastically after the length exceeded 9m and dropped to zero after the length surpassed 17m; the steel-plastic geogrid (B6) obeyed the same strain distribution as that in test area A, whose strain approached zero after the geogrid length surpassed 17m. The results show that, despite the difference between the test areas and geogrids in strain distribution, the ultimate effective length of the geogrids in the pull-out tests was about 17m in both test areas.

(4) Through comparison, it is learned that the two test areas had basically the same pull-out load, ultimate effective length and strain, and shared similar laws of pull-out displacement, pull-out load and strain. It can thus be concluded that the fill

height has little impact on the pull-out properties of geogrids when the fill slopes have similar gradients and reach a certain height.

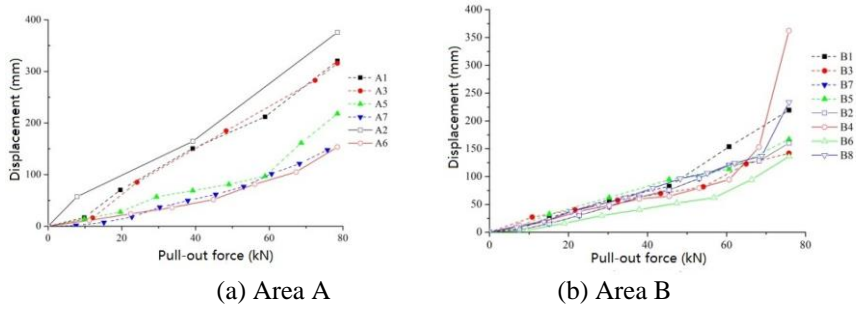


Figure 5. Relationship curve between pull-out force and pull-out displacement

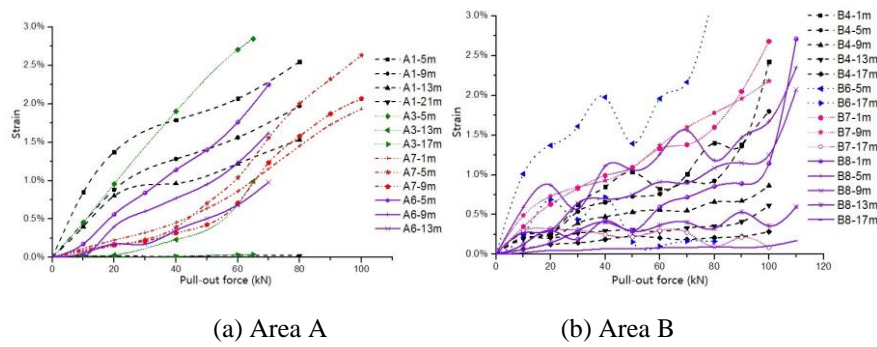


Figure 6. Relationship curve between pull-out force and strain in in-situ pull-out tests

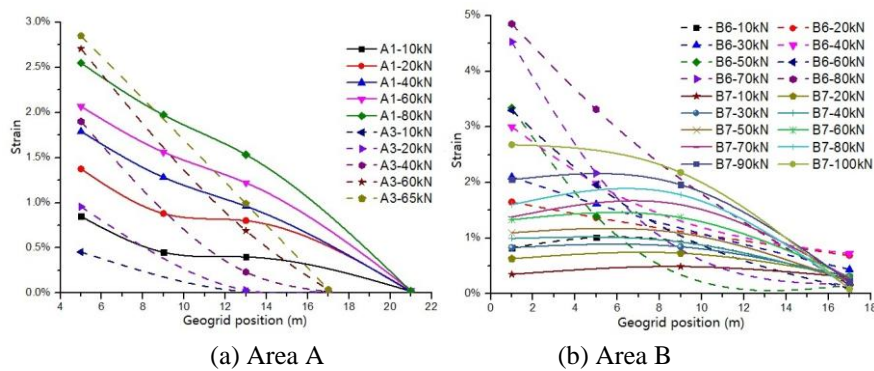


Figure 7. Relationship curve between strain and geogrid position in in-situ pull-out tests

5. Theoretical analysis

5.1. Theoretical derivation

If a geogrid is sufficiently long, the pull-out force will achieve equilibrium with the SRI friction when the tensile force F is smaller than the ultimate pull-out force. Since the geogrid is not in the extreme equilibrium state, the SRI friction cannot be described by the Mole/Coulomb's Law. Considering the laws revealed in the previous tests, it is assumed that the relationship between strain and position can be depicted by the S-curve:

$$\varepsilon(x) = \frac{A_1 - A_2}{1 + e^{\frac{x-x_0}{A_3}}} + A_2 \quad (1)$$

It is obvious that $\varepsilon(+\infty) = 0$. Substituting $\varepsilon(+\infty) = 0$ into equation (1), we have $A_2 = 0$. Since $\varepsilon(0) = F/E$, we have $A_1 = \frac{F}{E}(1 + e^{-x_0/A_3})$ (The geogrid is assumed to be in the linear elastic range with the elastic modulus of E). Let L_e be the effective length of the geogrid at the current moment. Substituting $A_1 = \frac{F}{E}(1 + e^{-x_0/A_3})$ into equation (1), the strain, shear stress and displacement can be obtained as:

$$\left\{ \begin{array}{l} \varepsilon(x) = \frac{\frac{F}{E}(1 + e^{-x_0/A_3})}{1 + e^{\frac{x-x_0}{A_3}}} \\ \tau(x) = -\frac{E}{2A} \frac{\partial \varepsilon(x)}{\partial x} = \frac{A_1 E}{2AA_3} \frac{e^{\frac{x-x_0}{A_3}}}{(1 + e^{\frac{x-x_0}{A_3}})^2} = \frac{F(1 + e^{-\frac{x_0}{A_3}})}{2AA_3} \frac{e^{\frac{x-x_0}{A_3}}}{(1 + e^{\frac{x-x_0}{A_3}})^2} \\ \Delta L = \int_0^{L_e} \varepsilon(x) dx = \frac{F}{E} (1 + e^{-x_0/A_3}) (L_e + A_3 \ln \frac{1 + e^{-\frac{x_0}{A_3}}}{1 + e^{-\frac{L_e-x_0}{A_3}}}) \end{array} \right. \quad (2)$$

where $\varepsilon(x)$ is equal to or greater than zero and monotonically decreasing; L_e is theoretically infinitely great. It is assumed that L_e is the root corresponding to $\varepsilon(x) = \delta(\varepsilon)$ ($\delta(\varepsilon)$ is a small value greater than zero). If neither A_3 nor x_0 is related to position and the pull-out force, it can be inferred from equation (2) that the pull-out force is linearly correlated with the strain and pull-out displacement at any position. The results are basically consistent with the data obtained from in-situ pull-out tests.

Since the L_e is theoretically infinitely great and the strain is decreasing to zero, the pull-out displacement ΔL ought to converge to a certain value:

$$\begin{aligned}\Delta L &= \lim_{L_e \rightarrow +\infty} \frac{F}{E} (1 + e^{-x_0/A_3}) (L_e + A_3 \ln \frac{1 + e^{\frac{x_0}{A_3}}}{1 + e^{\frac{L_e - x_0}{A_3}}}) \\ &= A_1 A_3 \ln(1 + e^{\frac{x_0}{A_3}}) + A_1 x_0\end{aligned}\quad (3)$$

Obviously, the pull-out displacement can be determined when the pull-out force is constant and the two factors have a linear relationship. Figure 8 illustrates how strain and shear stress change with the geogrid positions. As shown in the figure, the strain gradually decreases with the increase of the distance to the slope surface, which agrees with the actual condition. When $x_0 > 0$, the shear stress first increases and then decreases. This is because the overburden pressure is small near the slope surface, and the friction in the pull-out process mainly comes from the cohesion between soil and reinforcement. With the increase of the distance to the slope surface, the overburden pressure increases gradually; the growth in the normal stress gives play to the effect of the internal friction angle, which pushes up the shear stress. Further growth in the distance to the slope surface suppresses the rib strain and thus the shear stress. As a result, the shear stress increases first and then decreases (Figure 8(a)). When the internal friction angle is zero ($x_0 = 0$), the cohesion is the only force present; thus, the shear stress decreases monotonically (Figure 8(b)). In addition, when the cohesion ceases to exist, the shear stress on the slope surface is zero, and then increases before the eventual decline.

According to the function images and analytic expressions of strain and shear stress, the peak shear stress will shift to the right with the increase in the internal friction angle, the slope ratio, and the filler bulk density, and to the left with the increase in the cohesion; the growth in pull-out force F will cause the increase of the effective geogrid length. According to the functional relationship between strain and shear stress, the shear stress function will shift to the right with the increase of x_0 , and the effective geogrid length will grow with the increase of A_3 and F . Hence, the internal friction angle, the slope ratio, and the filler bulk density are all negatively correlated with A_3 and x_0 ; the cohesion is negatively correlated with A_3 but positively with x_0 . Through the above analysis, the empirical formula for A_3 and x_0 can be derived from the data of in-situ tests:

$$\begin{cases} A_3 = \frac{\ln(c + \gamma a \tan \varphi + 1)}{A a^{2.2} (c + \gamma a \tan \varphi + 1)} \\ x_0 = \begin{cases} \frac{\sqrt{\gamma a \tan \varphi - cA}}{2A^{0.5} a^{0.2}}, & \gamma a \tan \varphi \geq cA \\ 0, & \gamma a \tan \varphi < cA \end{cases} \end{cases}\quad (4)$$

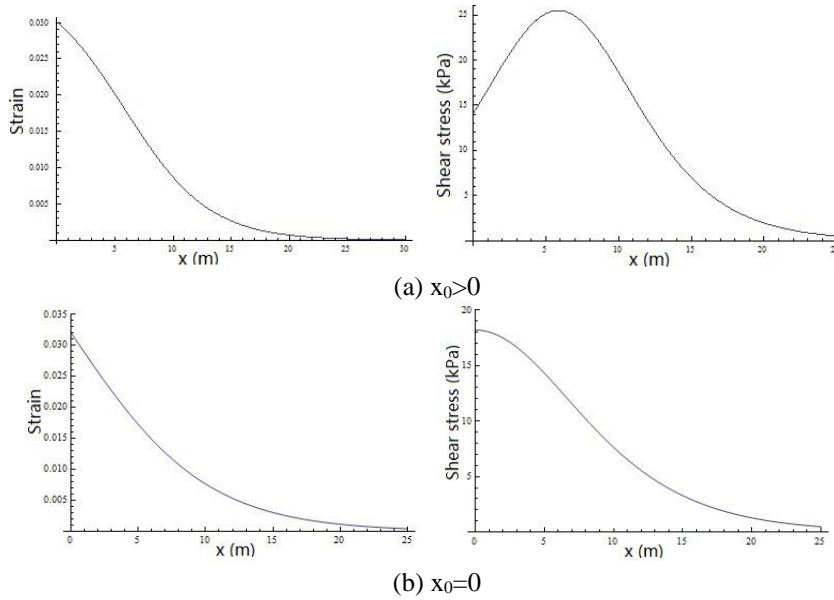


Figure 8. Variation in strain and shear stress with geogrid positions

5.2. Theoretical calculation

The in-situ pull-out test data were computed and analysed to verify the above theories. The test area A was taken as the example to explain the relationship curves between pull-out force and pull-out displacement (Figure 9), between geogrid position, strain and SRI shear stress (Figure 10), between pull-out force and strain (Figure 11), and between pull-out force and SRI shear stress (Figure 12).

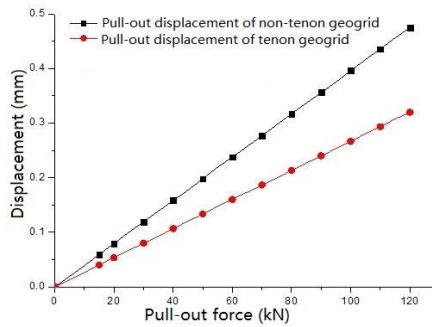


Figure 9. Relationship curve between pull-out force and pull-out displacement

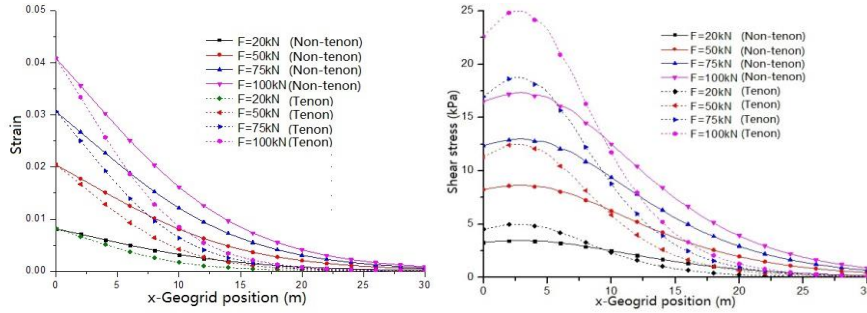


Figure 10. Relationship curve between geogrid position, strain and SRI shear stress

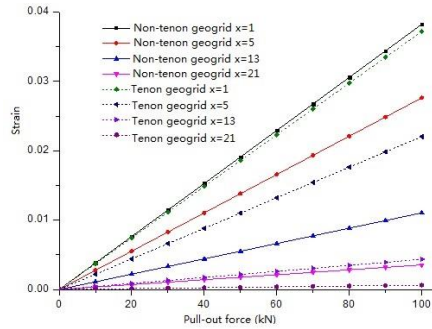


Figure 11. Relationship curve between pull-out force and strain

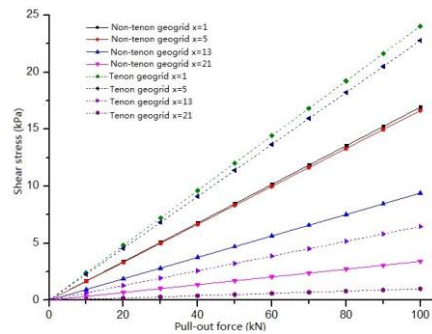


Figure 12. Relationship curve between pull-out force and SRI shear stress

As shown in Figure 9, the pull-out force is linearly correlated with the pull-out displacement, which is in line with the test situation (Figure 5). It can be seen from

Figure 10 that, when the pull-out force was constant, the strain entered a gradual, nonlinear decrease, while the shear stress increased before decreasing with the increase in the distance to the slope surface. These trends are consistent with the actual situation (Figures 6 and 7).

Figures 11 and 12 show that, when the position was constant, the geogrid strain and SRI shear stress increased linearly with the growth in the pull-out force, and the growth rates of strain and stress were decreasing with the increase of the distance to the slope surface. These phenomena agree well with the test results (Figures 6 and 7).

5.3. Comparison with in-situ pull-out tests

In the in-situ pull-out tests, the geogrids were too sparse in some places rather than paved evenly across the test areas; the fillers were uneven and anisotropic; the barrier strips of the geogrids interacted with each other. Under these unfavourable conditions, the ribs were subjected to unbalanced tensile forces during the pull-out tests, leading to discreteness in stress, strain and displacement at many positions. The geogrids were broken one by one rather than damaged at once. As a result, the single-rib strength acquired from the tests was smaller than that obtained from indoor tests. Since the damaged geogrids must have reached the ultimate strength, the in-situ test data should be modified properly to ensure its rationality.

For the relationship between the pull-out force and the pull-out displacement, the ultimate pull-out force of the in-situ tests was converted into the ultimate strength of indoor tests (75.8kN/m), and the other pull-out forces were multiplied by the corresponding coefficient. The pull-out force and pull-out displacement values thus obtained for the in-situ tests and the theoretical values are given in Figure 13. Obviously, the theoretical values of test area A fell in the range of in-situ test data and near the mean values, while those of test area B deviated greatly from the measured data.

Based on the test results on A7 and B4, the theoretical relationship between pull-out force and strain was compared with that observed in the test. The comparison is shown in Figure 14, where the pull-out force has been modified by the said method. It can be seen that the strain and pull-out force measured at the same position had a linear relationship. The theoretical relationship agrees well with the measured relationship. In fact, the relationship between the pull-out force and strain at any position in the pull-out tests can be described as a linear relationship, which is consistent with the previous theories.

Based on the test results on B4, the theoretical relationship between strain and position at a given pull-out force was compared with that observed in the test. According to the comparison in Figure 15, the theoretical trends of these factors were the same with those reflected by the measured data, and the error between theoretical and measured results was rather small. This validates the theories drawn in the previous section. In fact, most of the pull-out test data are basically consistent with the basic theoretical laws (function image). Only a few data have some deviations. For example, the strain of B7 and B8 increased with the depth. The

abnormality may be attributed to the local bending and slacking of the geogrids in the construction process.

To sum up, the theoretical laws are consistent with those reflected in the in-situ test data. of course, some of the theoretical data differ greatly from the measured data. There are two possible reasons for the difference: First, our theories are not perfect and some parameters are not rational enough; second, the field conditions are complex and constantly changing, and disturbances and damages may occur due to construction and testing.

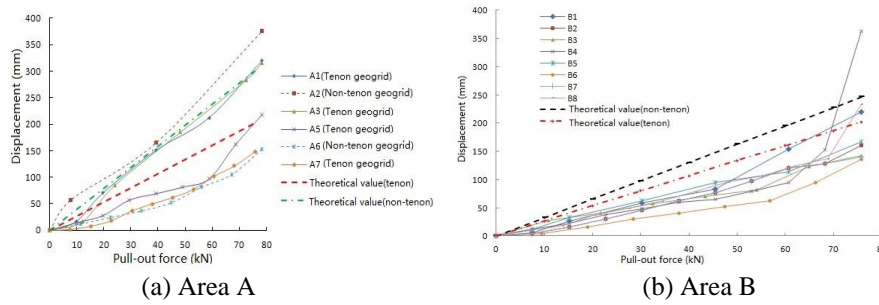


Figure 13. Comparison between theoretical and measured relationships between pull-out force and pull-out displacement

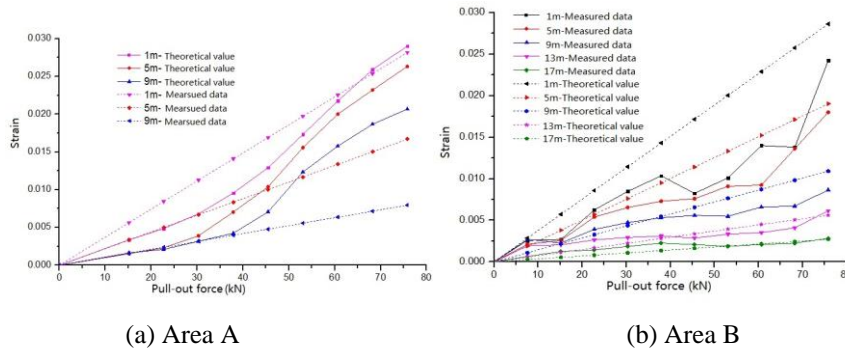


Figure 14. Comparison between theoretical and measured relationships between pull-out force and strain

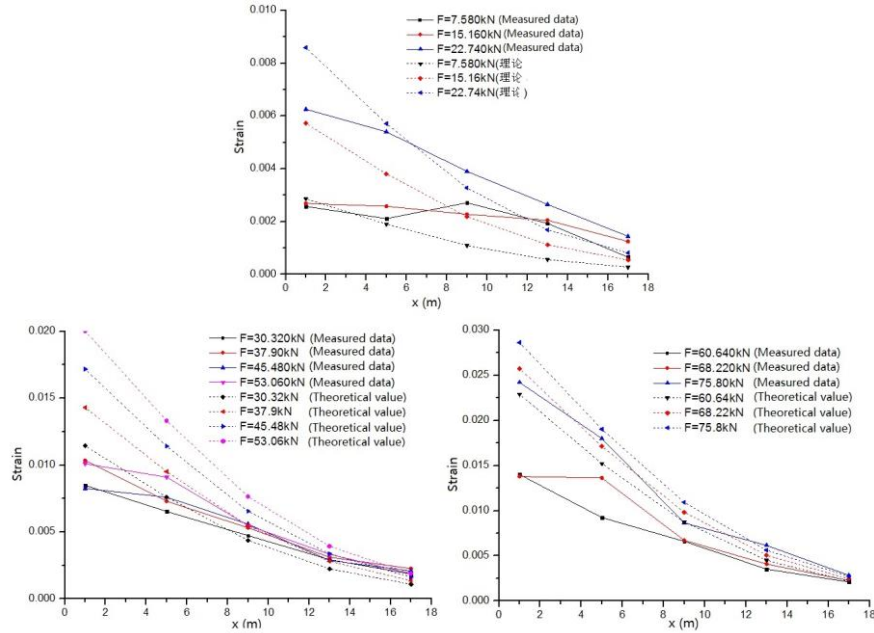


Figure 15. Comparison between theoretical and measured relationships between strain and position (B4)

6. Conclusions

The in-situ test results show that, under any pull-out action, the pull-out load has a near linear relationship with the pull-out displacement and the strain, while the strain and stress decrease nonlinearly with the distance from the geogrid to the slope surface.

Assuming that the relationship between strain and position is an S-curve, the effective length and pull-out displacement of geogrids were computed at different pull-out forces according to the data acquired through indoor tests and in-situ pull-out tests. Through the comparison against the test results, it is proved that the S-curve model outputted basically the same laws with those observed in the tests. Thus, the calculation and theories of our research are rational and valid.

References

- Bakeer R. M., Sayed S. M., Cates P., Subramanian R. (1998). Pullout and shear tests on geogrid reinforced lightweight aggregate. *Geotextiles & Geomembranes*, Vol. 16, No. 2, pp. 119-133. [http://dx.doi.org/10.1016/S0266-1144\(97\)10025-5](http://dx.doi.org/10.1016/S0266-1144(97)10025-5)

- Chen J. F., Li H. L. (2009). Status and prospect of research on geosynthetics/soil interface properties. *Journal of underground space and Engineering*, Vol. 5, No. 5, pp. 1049-1054.
- Chen R., Luan M. T., Zhao W., Xu X. Y., Han D. X. (2009). Studies on pullout test and frictional resistance characteristic of geogrids. *Rock and Soil Mechanics*, Vol. 30, No. 4, pp. 960-964.
- Liu H., Li P. F., Zhang Z. Y., Han W. X. (2004). Asystem atic research on the deformation and stability of high embankment of airport in mountainous area. *Advance In Earth Sciences*, Vol. 19, No. S1, pp. 324-328.
- Liu X., Tang X. W., Shen H., Gao B. S. (2013). Stress distribution of reinforcement of reinforced soil structures under drawing force. *Chinese Journal of Geotechnical Engineering*, Vol. 47, No. 4, pp. 800-804.
- Liu Z., Huang X. J., Yang G. L. (2011). Study of combined panel earth retaining wall reinforced with double twisted hexagonal wire mesh by using site test. *Rock and Soil Mechanics*, Vol. 32, No. 11, pp. 3295-3300.
- Meng F. X., Xu C. (2009). Comparison and analyses of direct shear test and pull-out test of the interface between soils and geosynthetics. *Hydrogeology & Engineering Geology*, Vol. 36, No. 6, pp. 80-84. https://dx.doi.org/10.1007/978-3-540-85168-4_52
- Mo J. Z., He G. C., Wang C. Z., Zhou S. L. (2008). Study on a stepped retaining wall with geogrid reinforcement by using site test and numerical analysis. *China Civil Engineering Journal*, Vol. 41, No. 5, pp. 52-58.
- Shi D. D., Liu W. B., Shui W. H., Liang Y. H. (2009). Comparative experimental studies of interface characteristics between uniaxial/biaxial plastic geogrids and different soils. *Rock and Soil Mechanics*, Vol. 30, No. 8, pp. 2237-2244. <https://dx.chinadoi.cn/10.3969/j.issn.1000-7598.2009.08.006>
- Wang D. Y., Gao C., Wang C. Z., Han C., Tong Y. (2016). Rules of load transfer between soil and reinforcement in reinforced earth retaining wall with sandy cobble. *Journal of Yangtze River Scientific Research Institute*, Vol. 33, No. 7, pp. 105-109.
- Wang R., Wang S., Peng D. L. (2016). Steel-Plastic tenon geogrid and its interaction characteristics with backfills. *Journal of Engineering Geology*, Vol. 24, No. 3, pp. 391-397.
- Yang G. Q., Zhou Y. T., Zhou Q. Y. (2013). Distribution rules of axial stress of reinforcement in reinforced earth retaining wall. *Chinese Journal of Geotechnical Engineering*, Vol. 47, No. 4, pp. 650-654. <https://dx.chinadoi.cn/10.3969/j.issn.0254-5071.2000.04.014>
- Yang G. Q., Zhou Y. T., Zhou Q. Y., Xue X. H. (2009). Experimental research on geogrid reinforced earth retaining wall. *Rock and Soil Mechanics*, Vol. 30, No. 1, pp. 206-210.
- Zhang F. (2008). Field test research on geogrid reinforced earth high retaining wall. *China Railway Science*, Vol. 29, No. 4, pp. 1-7.